CD36-Mediated Hematoma Absorption following Intracerebral Hemorrhage: Negative Regulation by TLR4 Signaling

Huang Fang,* Jing Chen,* Sen Lin,[†,‡] PengFei Wang,* YanChun Wang,* XiaoYi Xiong,* and QingWu Yang*

Promoting hematoma absorption is a novel therapeutic strategy for intracerebral hemorrhage (ICH); however, the mechanism of hematoma absorption is unclear. The present study explored the function and potential mechanism of CD36 in hematoma absorption using in vitro and in vivo ICH models. Hematoma absorption in CD36-deficient ICH patients was examined. Compared with patients with normal CD36 expression, CD36-deficient ICH patients had slower hematoma adsorption and aggravated neurologic deficits. CD36 expression in perihematomal tissues in wild-type mice following ICH was increased, whereas the hematoma absorption in $CD36^{-/-}$ mice was decreased. $CD36^{-/-}$ mice also showed aggravated neurologic deficits and increased TNF-α and IL-1β expression levels. The phagocytic capacity of $CD36^{-/-}$ microglia for RBCs was also decreased. Additionally, the CD36 expression in the perihematoma area after ICH in $TLR4^{-/-}$ and $MyD88^{-/-}$ mice was significantly increased, and hematoma absorption was significantly promoted, which was significantly inhibited by an anti-CD36 Ab. In vitro, TNF-α and IL-1β significantly inhibited the microglia expression of CD36 and reduced the microglia phagocytosis of RBCs. Finally, the TLR4 inhibitor TAK-242 upregulated CD36 expression in microglia, promoted hematoma absorption, increased catalase expression, and decreased the H_2O_2 content. These results suggested that CD36 mediated hematoma absorption after ICH, and TLR4 signaling inhibited CD36 expression to slow hematoma absorption. TLR4 inhibition could promote hematoma absorption and significantly improve neurologic deficits following ICH. ***The Journal of Immunology*****, 2014, 192: 5984–5992.**

Hematomas form when blood enters the cerebral parenchyma after an intracerebral hemorrhage (ICH); hematomas are the primary cause of neurologic deficits associated with ICH. The early stages of hematoma compression cause deformation and mechanical injury to local brain tissues. Secondary neuronal damage is caused by direct toxicity and inflammatory responses induced by the components and metabolic products of late-stage hematomas and aggravates neurologic deficits (1). Therefore, effective hematoma removal is a goal of ICH treatment, as hematoma removal can relieve mechanical compression, limit inflammatory injury, and promote the recovery of neuronal function (2–4). Clinically, the rate of hematoma absorption in patients with ICH correlates with the degree of neurologic deficit (5); however, the mechanism underlying hematoma absorption remains unknown.

Scavenger receptors play important roles in the regulation of phagocytosis in macrophages (6). CD36 is a type II scavenger receptor that can bind to modified lipids, symmetric red cell ghosts, or apoptotic neutrophils; this receptor plays an important role in mediating phagocytosis (7, 8). Cells lacking phagocytic abilities acquire phagocytic functions following transfection with CD36 (9, 10). A peroxisome proliferator-activated receptor γ agonist promotes hematoma absorption following ICH, which significantly reduces secondary inflammatory damages; the mechanism may be associated with the upregulation of CD36 expression in the microglia (2). However, the function of CD36 and the regulatory mechanism underlying the effect of CD36 in hematoma absorption are unclear.

TLRs are important components of the innate immune system that recognize pathogen- and damaged-associated molecular patterns that could induce inflammatory responses (11). Many studies have demonstrated that TLR4 participates in the development of sterile inflammation and plays an important role in the inflammatory responses of the CNS, such as those that occur in the case of cerebral ischemia and Parkinson's disease (12). Our previous studies showed that TLR4 activation following ICH results in NF-κB activation via the MyD88 pathway, resulting in the production of large quantities of inflammatory factors, such as TNF-α and IL-1β; these factors may cause inflammatory damage and aggravate neurologic deficits (13). Treatment with the TLR4 inhibitor ethyl (6*R*)-6-[*N*-(2-chloro-4-fluorophenyl)sulfamoyl]-cyclohex-1-ene-1-carboxylate (TAK-242; Takeda Pharmaceutical Company, Osaka, Japan) decreases secondary inflammatory damage following ICH (14). Other studies have shown that inflammatory factors such as TNF-α, which is induced by the activation of TLR signaling pathways, downregulate the expression of CD36 in macrophages and

*Department of Neurology, Xinqiao Hospital, Third Military Medical University, Chongqing 400037, China; [†]Department of Development and Regeneration Key Laboratory of Sichuan Province, Chengdu Medical College, Chengdu 610083, China; and [‡]Department of Histoembryology and Neurobiology, Chengdu Medical College, Chengdu 610083, China

Received for publication January 10, 2014. Accepted for publication April 5, 2014.

This work was supported by National Natural Science Foundation of China Grant 81271283 and National "973" Project Grant 2014CB541605.

Address correspondence and reprint requests to Prof. QingWu Yang, Department of Neurology, Xinqiao Hospital, Third Military Medical University, 183 Xinqiao Main Street, Shapingba District, Chongqing 400037, China. E-mail address: yangqwmlys@hotmail.com

The online version of this article contains supplemental material.

Abbreviations used in this article: CT, computerized tomography; GFAP, glial fibrillary acidic protein; ICH, intracerebral hemorrhage; mRS, modified Rankin Scale; NDS, neurological deficit score; NIHSS, National Institutes of Health Stroke Scale; TAK-242, ethyl (6*R*)-6-[*N*-(2-chloro-4-fluorophenyl)sulfamoyl]cyclohex-1-ene-1-carboxylate; WT, wild-type.

affect cellular phagocytic functions that are essential to infection-related inflammatory responses (15). Additionally, CD36 expression in perihematomal tissues is significantly upregulated in TLR4$^{-/-}$ mice subjected to ICH (16). Therefore, we hypothesized that CD36 mediates hematoma absorption following ICH and that the activation of TLR4 signaling following ICH produces inflammatory factors such as TNF-α that could downregulate CD36 expression and mediate hematoma absorption. To understand the involvement of CD36 and TLR4 signaling in hematoma absorption following ICH, we modified CD36 expression in the relevant cells. The goal of the present study was to further understand the regulatory mechanism underlying hematoma absorption following ICH to identify treatment options that promote hematoma absorption in patients with ICH.

Materials and Methods

Clinical study

Certain people have CD36 expression deficiencies that affect the development of atherosclerosis (17, 18). To evaluate the effect of CD36 deficiency on hematoma absorption and neurologic deficits, we screened patients with ICH for CD36 expression. Between July 2012 and June 2013, 209 patients with ICH were identified. The inclusion criteria were as follows: 1) the patient was identified within 24 h of disease onset; 2) the patient must not have had a previous ICH, and the hemorrhage in the basal ganglia had to be confirmed by cranial computerized tomography (CT); and 3) the hematoma must not have ruptured into the cerebral ventricles. The exclusion criteria were as follows: 1) the patient was <18 y or >80 y old; 2) the patient chose to undergo surgical treatment; 3) the patient was in a coma or died within 48 h of the ICH; 4) the ICH was caused by a brain tumor, trauma, drug abuse, coagulation abnormalities, anticoagulation therapy, or vascular malformations; 5) the patient had had an obvious inflammatory disease 6 mo prior to enrollment (e.g., acute or chronic infectious diseases, systemic lupus erythematosus, rheumatism, or rheumatoid disease); 6) the patient had a nosocomial infection; 7) the patient had an acute myocardial infarction; 8) the patient had acute or chronic liver damage; and 9) the patient was not compliant with the study protocol or could not undergo all of the tests required by the study. A total of 10 patients were excluded from the study, including 3 patients who died and 7 who were lost to follow-up. A total of 199 patients met the inclusion criteria and were enrolled in the study. Upon admission to the hospital, 10 ml blood from the median cubital vein was collected to screen for CD36 deficiency. A cranial CT scan was performed on the day of admission and 7 d after admission, as the hemorrhaged clot is generally hyperdense relative to adjacent healthy cerebral parenchyma in the early subacute phase of ICH (19, 20). The hematoma was visualized by CT scanning (64-slice CT machine; Siemens, Munich, Germany). Hemorrhage volumes were measured via computerized planimetry. The measurement of hemorrhage volume by planimetrics is an established and accurate method that uses computer-assisted image analysis (21). The volumes were expressed in cubic centimeters. The volumes of hemorrhages within the ventricular system were not measured. The following parameters were used for all CT studies: section thickness, 5 mm; gap, 5 mm; pitch, 1; tube current, 304 mA; and voltage, 120 kV. The hematoma absorption rate (percentage) was calculated with the following formula: [(hematoma volume at 7 d − hematoma volume at admission)/hematoma volume at admission] × 100. On admission and 7, 14, and 30 d after admission, the patients were evaluated using the National Institutes of Health Stroke Scale (NIHSS). Modified Rankin Scale (mRS) scores were used to evaluate neurologic deficits in patients 3 mo after the onset of the ICH (22).

CD36 screening was performed using a sequence-specific primer PCR assay. CD36 mutant primers were designed using information from previous reports (23, 24). These mutations are the most common mutations that cause CD36 expression defects in Asian populations (Supplemental Table I). The patients lacking positive bands in the electrophoretogram were considered CD36 deficient (Supplemental Fig. 1A). The mutations were confirmed through sequencing analysis (data not shown). The types of CD36 deficiency were identified through Western blot analysis of monocytes (Supplemental Fig. 1B). Eleven patients with CD36 deficiency in monocytes were identified (type I deficiency). Eleven patients with normal CD36 expression had similar hematoma volumes at the same sites and were selected to form the control group. Both groups of patients had similar baseline data. The clinical data of the patients in these two groups are shown in Supplemental Table II.

Collection of human brain tissue

Brain tissue samples from ICH patients were collected from the brain bank of the Department of Neurosurgery of Xinqiao Hospital of the Third Military Medical University (Chongqing, China). All autopsies had been performed within 24 h of death. The inclusion criteria were as follows: 1) the patient must not have had a previous ICH, and hemorrhage in the basal ganglia was confirmed by CT scan; and 2) the patient had died within 48 h of disease onset. The exclusion criteria were as follows: 1) the patient had a traumatic hemorrhage or a hemorrhage caused by a coagulation dysfunction; 2) the patient had a history of acute or chronic infection or a known inflammatory or autoimmune disease; and 3) the patient had a tumor, cachexia, or had used immunosuppressive drugs for a prolonged period of time. Three patients met the inclusion criteria and were enrolled. After the human brain tissues were collected at autopsy, the perihematomal tissues were used to detect CD36 expression using immunofluorescence. This protocol for the clinical study was approved by the Ethics Committee of the Xinqiao Hospital of the Third Military Medical University. All of the subjects or authorized relatives signed informed consent forms. This study did not have any medical ethics–related issues.

Animals

C57BL/6 mice (male, 8–10 wk old, 20–24 g) were obtained from the Animal Center of the Third Military Medical University. TLR4$^{-/-}$, MyD88$^{-/-}$, and CD36$^{-/-}$ mice were purchased from The Jackson Laboratory (Bar Harbor, ME). All of the knockout mice had maintained the C57BL/6 genetic background over the course of six generations of hybridization, and all were identified using appropriate methods. The mice were housed in a clean environment and given ad libitum access to food and water. The experimental protocol was approved by the Animal Management Committee of the Third Military Medical University. The mice were randomly divided into groups, and the investigators were blinded to the group allocation of the mice.

ICH model

The establishment of the ICH model has been described previously (14). Briefly, the mice were anesthetized with 4% chloral hydrate and immobilized in a stereotactic apparatus (Stoelting, Wood Dale, IL). Twenty microliters blood was collected from the tail vein, then directly injected into the striatum without anticoagulant through stereotactic apparatus at 0.8 mm anterior and 2 mm lateral (on the left side) to the bregma and at a depth of 3.5 mm. The blood was injected at a speed of 2 μl/min. The needle was maintained in place for 10 min until the blood had coagulated; the microinjector was then removed. The skull was sealed with bone wax, and the scalp was sutured. The rectal temperature was maintained at ~37°C; after recovery, the mice were given free access to water and food. In parallel, sham mice received 20 μl striatal saline injection and were subjected to the same manipulations as the ICH mice. The success rate of the model was 90%; failed models and dead mice were excluded from this study.

Analysis of the neurologic deficit score

The experiment was performed as described previously (14), and a 28-point neurologic deficit scale was adopted. Circling behavior, climbing, front limb symmetry, and body symmetry were assessed. The scoring was performed by two blinded laboratory investigators who were unaware of the mouse groupings. The average score was the final score of each mouse.

Hematoma measurement

As in our previous report (25), the mice were anesthetized using a lethal dose of chloral hydrate. After perfusion and fixation, the brains were removed and sectioned from the frontal lobe to the occipital lobe to prepare coronal brain sections with a thickness of 1 mm. The fixed brain sections were sequentially arranged, and Image-Pro Plus 5.0 image processing software (Media Cybernetics, Bethesda, MD) was used to measure the ICH volume (cubic millimeters). The hematoma volume was calculated using the formula $V = t \times (A2 + \ldots + An)$, where V is the hematoma volume, t is the section thickness, and A is the bleeding area. Additionally, the hemoglobin content in the brain tissues was measured to further quantify hematoma size (2). Blood (0, 2, 4, 8, 16, and 20 μl) was added to fresh brain homogenates, and OD was then measured and recorded at 540 nm using a spectrophotometer (Thermo Multiskan, Pittsburgh, PA). The obtained values were used to prepare the standard curve. The striatum was removed after the ICH was initiated and dissolved in Drabkin's reagent. The supernatant of the homogenate was collected and measured using

a spectrophotometer; the hematoma volume (microliters) was then calculated using the standard curve.

Brain water content

As previously described (14), we randomly selected mice from each group to measure the brain water content at 3 d after the model was successfully constructed ($n = 6$). Briefly, the mice were anesthetized by i.p. injection, and the cerebral tissues were removed. The samples were divided into five parts: the ipsilateral cortex, the ipsilateral basal ganglia, the contralateral cortex, the contralateral basal ganglia, and the cerebellum. The brain water content (percentage) was calculated with the formula [(wet weight − dry weight)/wet weight] × 100.

Immunohistochemical staining

Following our previous methods (13), human and mouse perihematomal tissues were fixed in 4% paraformaldehyde. The samples underwent gradient dehydration, embedding, freezing, and sectioning into 20-μm-thick sections; CD36 expression was detected using double fluorescence immunohistochemistry. The following primary Abs were used in this experiment: mouse anti-human CD36 (1:200; LifeSpan, Seattle, WA), rabbit anti-human Iba-1 (1:200; Wako Pure Chemical Industries, Osaka, Japan), rabbit anti-human NeuN (1:200; Millipore, Darmstadt, Germany), rabbit anti-human glial fibrillary acidic protein (GFAP; 1:100; Dako, Glostrup, Denmark), rabbit anti-mouse CD36 (1:200; Abcam, Cambridge, U.K), rat anti-mouse CD11b (1:200; Millipore), mouse anti-mouse GFAP (1:100; Cell Signaling Technology, Danvers, MA), and mouse anti-mouse NeuN (1:100; Millipore). The secondary Abs included Alexa Fluor 647 (1:200; donkey anti-mouse), Alexa Fluor 594 (1:200; donkey anti-rabbit), and Alexa Fluor 488 (1:200; donkey anti-rabbit, donkey anti-mouse, and donkey anti-rat, all from Invitrogen, Carlsbad, CA). The observed results were imaged by confocal microscopy (LSM 780, Carl Zeiss, Jena, Germany, and TCS Sp5, Leica, Mannheim, Germany).

Real-time quantitative RT-PCR

Tissue and cellular RNA was extracted using the TRIzol reagent (Invitrogen, Gaithersburg, MD), and cDNA was synthesized using the iScript cDNA synthesis reagent (Bio-Rad, Hercules, CA) according to the manufacturers' instructions. Real-time quantitative RT-PCR was performed in a 96-well plate in the Bio-Rad iQ PCR machine (Bio-Rad, Hercules, CA) with the iQ SYBR Green reagent. The primers were purchased from Shanghai Sangon Biotech. The primer sequences used in the study are shown in Supplemental Table I. The $2^{-\Delta\Delta CT}$ method was used to calculate relative gene expression levels (13).

Western blot

As in our previous report (14), proteins from perihematomal tissues or cultured microglia were resolved by SDS-PAGE and transferred onto polyvinylidene fluoride membranes by electroblotting. The membranes were incubated with mouse anti-human CD36 (for human blood, 1:400; Wako Chemicals USA, Richmond, VA) or rabbit anti-mouse CD36 (for perihematomal tissues and cells, 1:400; Abcam) at 4˚C overnight; GAPDH (1:400; Santa Cruz Biotechnology, Dallas, TX) was used as a loading control. The membranes were incubated with HRP-conjugated goat anti-mouse secondary Abs (1:2000) or HRP-conjugated goat anti-rabbit secondary Abs (1:2000; all from Sigma-Aldrich, St. Louis, MO) at 25˚C for 1.5 h. Bound Abs were visualized using a chemiluminescence detection system. The signals were measured by scanning densitometry and computer-assisted image analysis. Protein levels were calculated as the ratio of the values corresponding to the band of the detected protein to the values corresponding to the GAPDH band.

Microglial culture

Following methods described in the literature (2), the cells digested from the cerebral hemispheres of postnatal day 1 newborn mice were cultured for 2 wk. The loosely adherent microglia were harvested and inoculated into six-well plates or on 12-mm coverslips in 24-well plates at a concentration of 1×10^5 cells/ml. The experiment was performed on the following day. The cell purity was confirmed through immunohistochemistry using the microglia-specific rat anti-mouse CD11b Ab (1: 500; Millipore). The purity of the microglia was >95%.

Phagocytosis in vitro

Following previously described methods (2), we added mouse RBCs to cultures of microglia to model phagocytosis in vitro in a model of human ICH. Mouse RBCs were purified via density gradient centrifugation and labeled with CFSE (Invitrogen, Eugene, OR) for 30 min. RBCs were diluted to a concentration of 10^8 cells/ml, added to the cultured microglia in 24-well plates at a ratio of 10:1, and cultured for 12 h. The microglia were fixed and stained with rat anti-mouse CD11b (1:400; Millipore) followed by Alexa Fluor 594 (1:500, donkey anti-rat; Invitrogen, Carlsbad, CA) and Hoechst nuclear stain (Invitrogen, Eugene, OR). The observed results were visualized using confocal microscopy and imaged. The intracellular localization of RBCs (green fluorescence) was validated by Z-stack fluorescence confocal imaging. Briefly, Z-stack images were collected as a series of micrographs derived from different focal planes. Approximately 10 optical sections were captured from the top to the bottom of each section in our study. The internalized RBCs were observed surrounded by the red fluorescent cytomembrane of microglia when resectioning a Z-stack was performed. Green fluorescent RBCs bound to the surface were not surrounded by a red cytomembrane.

Flow cytometry

To detect the specific types of cells expressing CD36 in perihematomal tissues, single-cell suspensions of perihematomal tissues were prepared as described previously (16, 26). Briefly, after the mice were anesthetized with chloral hydrate, cardiac perfusion was performed using cold sterile PBS; the left brain was then removed immediately, placed in a C-tube (Miltenyi Biotec, Bergisch Gladbach, Germany), mixed with lysis buffer, and ground in a gentleMACS dissociator (Miltenyi Biotec). The brain tissue homogenate was filtered using a 40-μm sieve and incubated with demyelination microbeads at 4˚C for 15 min. An L magnetic column was used to separate the myelin sheath. The suspension that passed through the magnetic column was used to generate brain tissue single-cell suspensions. To explore the expression percentage of CD36 in each type of cell, the cells were stained with the relevant surface markers (anti-mouse CD36-PerCP-eFluor 710 [1:200; eBioscience, San Diego, CA), anti-mouse CD11b Ab–PE [1:200; Santa Cruz Biotechnology], and anti-mouse CD45 Ab–FITC (1:200; eBioscience]) for 30 min and fixed with Fix buffer (BD Biosciences, San Diego, CA) for 30 min at 4˚C. The cells were then incubated with BD Cytoperm and buffer for 10 min at room temperature and refixed for 10 min. The cells were then incubated with anti-mouse GFAP–Fluor 660 (1:200; eBioscience) and anti-mouse neuron-specific β-III tubulin PerCP (1:200; R&D Systems, Bingdon, U.K.) for 30 min at 4˚C. The data were collected with FACSDiva 6.0 flow cytometer software (BD Biosciences) and analyzed with FlowJo software (Tree Star, Ashland, OR). The microglia were marked by $CD45^{int}CD11b^{+}$, whereas neurons were identified as β-III $tubulin^{+}$, and astrocytes were identified as $GFAP^{+}$.

Analysis of phagocytosis of RBCs by microglia using flow cytometry

Following methods described in the literature (15), RBCs were stained with CFSE and combined with the cultured microglia at a ratio of 10:1. After coculturing for 12 h, the microglia were harvested and stained with anti–CD11b Ab-PE for 30 min. The flow cytometry analysis showed that all of the microglia were PE^{+}. The microglia that had engulfed RBCs were $PE^{+}CFSE^{+}$, and the nonengulfed RBCs in the supernatant were $CFSE^{+}$. Three indicators were used to assess the ability of microglia to phagocytize RBCs: 1) the percentage of microglia that had engulfed RBCs (the total number of $PE^{+}CFSE^{+}$ cells/all PE^{+} cells, expressed as percentage), 2) the average CFSE fluorescence intensity of microglia that had engulfed RBCs ($PE^{+}CFSE^{+}$), and 3) the number of nonengulfed RBCs ($CFSE^{+}$) in the supernatant. Additionally, changes in the microglia that had engulfed RBCs were observed using the CD36 Ab (5 μg/ml; Abcam).

Analysis of changes in microglial CD36 expression using flow cytometry

To investigate the changes of CD36 expression in $TLR4^{-/-}$, $MyD88^{-/-}$ microglia following ICH, CFSE-stained RBCs were added to the different microglial cultures at a concentration of 1×10^7 cells/ml and incubated for 12 h. To explore the different inflammatory factors on the influence of CD36 expression after ICH, CFSE-stained RBCs were added to the microglial cultures and incubated for 12 h in the presence of the vehicle, TNF-α (100 ng/ml; Life Technologies, Frederick, MD), IL-1β (100 ng/ml; R&D Systems, Minneapolis, MN), and IL-10 (10 ng/ml, BD Biosciences). The microglia were collected and stained with anti-mouse CD36-PerCP-eFluor 710 and anti-mouse CD11b Ab–PE for 30 min; the expression of CD36 and changes in the phagocytic ability of microglia were examined by flow cytometry.

TAK-242

TAK-242 (Takeda Pharmaceutical Company) is a TLR4-specific inhibitor (14). CFSE-stained RBCs were mixed and cocultured with microglia at

a ratio of 10:1 in the presence of TAK-242 (1 μmol/l), TAK-242 (1 μmol/l) plus TNF-α (100 ng/ml), TAK-242 (1 μmol/l) plus IL-1β (100 ng/ml), or vehicle (solution for producing TAK-242) for 12 h. CD36 expression and changes in phagocytosis in microglia were detected using flow cytometry. To observe the effect of TAK-242 on hematoma absorption following ICH, a previously described method was used (14); 6 h after the ICH model was successfully established, the mice were i.p. injected with TAK-242 (3 mg/kg, once per day for 5 d). The mice were divided into four groups: the sham group, the ICH plus vehicle group (the solvent for TAK-242, administered using the same volume as the TAK-242 group), the ICH plus TAK-242 group, and the ICH plus TAK-242 plus TNF-α group (first injecting TAK-242 and then immediately injecting 3 μg TNF-α). The mice were sacrificed 5 d later, and the volume of the hematomas was measured.

Detection of catalase mRNA and H_2O_2 concentrations

Following previously described methods (2), the microglial suspensions were divided into two groups: the vehicle group and the TAK-242 group. RBCs were added at a ratio of 10:1 in the presence of vehicle or TAK-242 (1 μmol/l). After culturing for 12 h, the microglia were collected and the changes in catalase mRNA expression were detected using quantitative PCR. The catalase primer was purchased from Shanghai Sangon Biotech, and the primer detail information is shown in Supplemental Table I. Additionally, the culture medium was collected and H_2O_2 concentrations were measured with a detection kit (Invitrogen) according to the manufacturer's instructions.

Statistical analyses

All of the data are presented as the means ± SD or the percentage. The analysis was performed using SPSS 16.0 software. A repeated two-way ANOVA was used to evaluate the differences in NIHSS scores for the clinical studies and in the neurologic deficit score (NDS) for animal studies between the groups and time points. The *t* test for independent samples or the Mann–Whitney *U* test was used to compare two groups; comparisons among multiple groups were examined using one-way ANOVA with a least significant difference post hoc test. Differences were considered significant when $p < 0.05$.

Results

CD36 affects hematoma absorption in ICH patients

The cranial CT images of patients in the CD36-deficient and CD36-normal groups on the day of admission and 7 d after admission showed that the hematoma volumes had changed (Fig. 1A). The difference in the hematoma volumes of CD36-deficient and CD36-normal patients was not significant at the onset of ICH; however, the hematoma volumes of the patients in the CD36-deficient group were larger than those of the patients in the CD36-normal group at 7 d after the onset of ICH (Fig. 1B). The hematoma absorption rate was lower in the CD36-deficient patients than in the CD36-normal patients (Fig. 1C). The NIHSS scores of CD36-deficient patients at 14 and 30 d were significantly higher than the scores of the CD36-normal patients (Fig. 1D); the mRS scores of the deficient patients at 90 d were also significantly higher than those of the normal patients (Fig. 1E). The results show that the hematoma absorption rate in CD36-deficient patients was reduced and that the neurologic deficits of these patients significantly aggravated their condition. This finding suggests that CD36 plays an important role in promoting hematoma absorption in patients with ICH.

CD36 expression following ICH

Changes in CD36 expression in the perihematomal region were observed using a mouse ICH model. At the corresponding time points, perihematomal tissues were collected (the field selections are shown in Supplemental Fig. 1C). The levels of CD36 mRNA and protein in the perihematomal tissues were significantly higher in the mice subjected to ICH than in the mice of the sham group. The expression levels peaked at 3 d after the onset of the ICH and then gradually decreased; on 7 d, the expression levels were still higher in the treated mice than in the sham mouse group (Fig. 2A, 2B). No time-dependent alterations in CD36 expression were observed in the sham group mice (data not shown). The results of

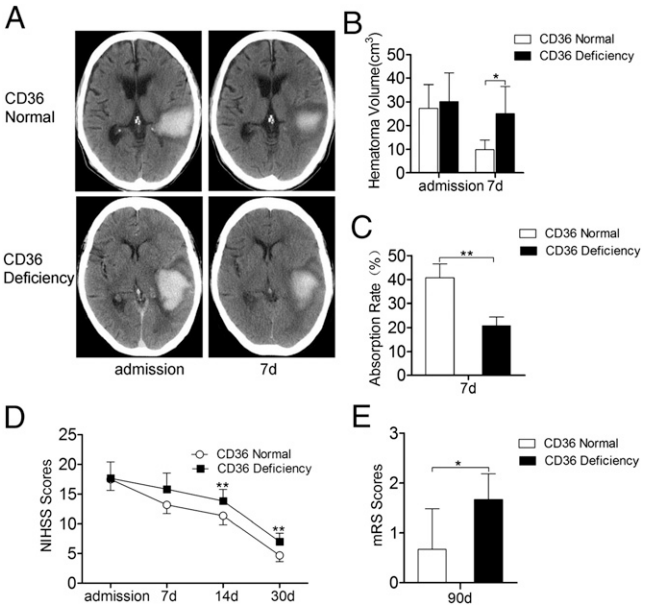

FIGURE 1. Reduced hematoma absorption and aggravated neurologic deficits in CD36-deficient patients with ICH. (**A**) Typical cranial CT images of CD36-normal ($n = 11$) and CD36-deficient ($n = 11$) ICH patients. Original magnification ×10. (**B**) Comparison of hematoma volumes in the CD36-deficient and CD36-normal groups at admission and 7 d after the onset of ICH. $*p < 0.05$ versus the CD36-normal group. (**C**) Decreased absorption rate in the CD36-deficient patients relative to the normal group. $**p < 0.01$ versus the CD36-normal group. (**D**) NIHSS scores and (**E**) mRS scores for ICH patients. $*p < 0.05$ versus the CD36-normal group, $**p < 0.01$ versus the CD36-normal group.

the flow cytometry analysis of cells from the perihematomal tissues showed that the expression levels of CD36 in neurons, astrocytes, and microglia were significantly higher in the experimental mice at 3 d after the onset of the ICH than in the sham group; however, microglia became $CD36^+$ at a significantly more rapid rate than did neurons and astrocytes (Fig. 2C). The immunofluorescent staining of perihematomal tissues from ICH patients produced results that were consistent with the results obtained with flow cytometry (Fig. 2D). Similarly, the results of immunofluorescent staining of the perihematoma of mice at 3 d after ICH were consistent with the patients who had experienced ICH (Supplemental Fig. 1D). As the resident phagocytes of the brain, microglia were involved in regulating the inflammatory response that occurs following ICH. Our results showed that CD36 was abundantly and mainly expressed in the microglia surrounding the perihematomal tissues following ICH, suggesting that CD36 plays a role in the pathological processes associated with ICH.

CD36-mediated hematoma absorption following ICH

The ICH model was used to evaluate the role of CD36 in the process of hematoma absorption. The absorption and the volume of hematomas were lower and larger, respectively, in $CD36^{-/-}$ mice than in wild-type (WT) mice (Fig. 3A, 3B). Additionally, the NDS and the brain water content of $CD36^{-/-}$ mice were significantly higher than those of the mice in the sham group (Fig. 3C, 3D); the mRNA levels of TNF-α and IL-1β were also higher in the perihematomal tissues of the $CD36^{-/-}$ mice than in the mice of the sham group. In contrast, IL-10 expression levels were significantly lower in the deficient mice than in the mice of the sham group (Fig. 3E).

To further confirm the involvement of CD36 in the promotion of hematoma absorption, we observed the phagocytosis of RBCs

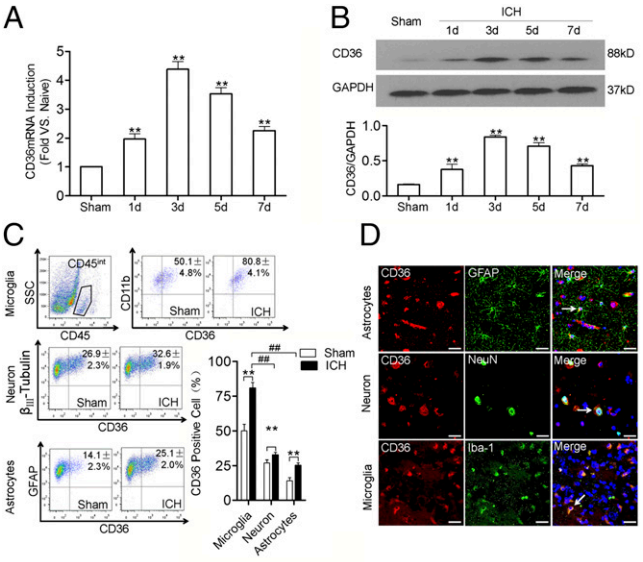

FIGURE 2. Enhanced CD36 expression in perihematomas following ICH. (**A**) Detection of CD36 mRNA expression in mice subjected to ICH using real-time quantitative RT-PCR. The data are expressed as fold increases relative to naive animals. $^{**}p < 0.01$ versus sham, $n = 6$. (**B**) Detection of CD36 protein expression in mice subjected to ICH using Western blot. $^{**}p < 0.01$ versus sham, $n = 6$. (**C**) Detection of CD36 expression in astrocytes, neurons, and microglia in the perihematomal tissues of mice using flow cytometry at 3 d after ICH. The *left panel* is the representative flow cytometry plot and the *lower right panel* is the percentage of $CD36^+$ cells in neurons, astrocytes, and microglia. Microglia were marked by $CD45^{int}CD11b^+$, whereas neurons were identified as β-III tubulin$^+$, and astrocytes were identified as $GFAP^+$. $^{**}p < 0.01$ versus sham, $^{\#\#}p < 0.01$ versus astrocytes or neurons, $n = 3$. (**D**) Detection of CD36 expression in human perihematomal tissues of ICH patients using fluorescence immunohistochemistry; CD36 expression was labeled with a CD36 Ab (red), astrocytes, neurons, and microglia were labeled with GFAP (green), Neun (green), and Iba-1 (green), respectively. The merged images of the overlay of CD36 together with astrocytes, neurons, and microglia were shown as yellow, and the nuclei were stained with DAPI (blue). The arrows indicate positive cells. Scale bars, 80 μm.

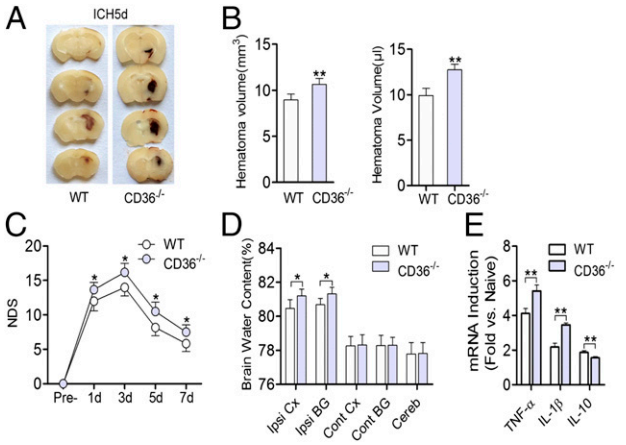

FIGURE 3. CD36-mediated hematoma absorption in mice with ICH. (**A**) Serial coronal sections of mouse brain tissues 5 d after the onset of ICH. Original magnification ×1.5. (**B**) Comparison of hematoma volumes between WT and $CD36^{-/-}$ mice. The data in the *left* and *right panels* are the Image-Pro Plus and hemoglobin detection results, respectively. $^{**}p < 0.01$ versus the WT group, $n = 6$. (**C**) The NDS of WT and $CD36^{-/-}$ mice at 1, 3, 5, and 7 d after the onset of ICH. $^{*}p < 0.05$ versus the WT group at the corresponding time points, $n = 6$. (**D**) Brain water content and (**E**) mRNA expression of inflammatory factors 3 d after the onset of ICH. The data in (E) were assessed by real-time quantitative RT-PCR and were expressed as fold increases relative to naive animals. $^{*}p < 0.05$ versus the WT group; $^{**}p < 0.01$ versus the WT group, $n = 6$. Cereb, cerebellum; Cont BG, contralateral basal ganglia; Cont CX, contralateral cortex; Ipsi BG, ipsilateral basal ganglia; Ipsi CX, ipsilateral cortex.

by different microglia in a simulated in vitro ICH model (2). Representative images showing the number of RBCs engulfed by microglia showed that significantly fewer RBCs were engulfed in the $CD36^{-/-}$ group than in the WT group. The ability to phagocytize RBCs was decreased in WT microglia treated with a CD36 Ab, whereas no change in the phagocytic ability of WT microglia treated with IgG was observed (Fig. 4A). Flow cytometry was conducted to analyze the ability of microglia to phagocytize RBCs; the $CD36^{-/-}$ group had significantly fewer PE^+CFSE^+ microglia that engulfed RBCs than did the WT group (Fig. 4B). Additionally, the average fluorescence intensity of CFSE in the PE^+CFSE^+ microglia was significantly decreased in the $CD36^{-/-}$ group (Fig. 4C). Accordingly, the number of nonengulfed RBCs in the supernatant was higher in the $CD36^{-/-}$ group than in the WT group (Fig. 4D). Similar results were observed when the microglia were treated with anti-CD36 Abs; in contrast, the phagocytosis of RBCs by microglia in the WT group was not significantly affected by treatment with IgG (Fig. 4B–D). These results suggest that CD36 plays an important role in promoting hematoma absorption.

TLR4/MyD88 signaling inhibits CD36 expression and decreases hematoma absorption

The effect of TLR4 signaling on CD36 expression and hematoma absorption was explored using in vitro and in vivo ICH models. CD36 expression in the perihematoma of the $MyD88^{-/-}$ and $TLR4^{-/-}$ mice was significantly increased at 3 d after the onset of ICH, as observed in the Western blot (Fig. 5A), and in the in vitro ICH model significantly increased CD36 expression was also detected in the $MyD88^{-/-}$ and $TLR4^{-/-}$ microglia by flow cytometry (Fig. 5B). Moreover, the significantly decreased hematoma volumes were found in the $MyD88^{-/-}$ and $TLR4^{-/-}$ mice (Fig. 5C), and flow cytometry showed that the $MyD88^{-/-}$ and $TLR4^{-/-}$ groups had more PE^+CFSE^+ microglia than did the WT group in vitro (Fig. 5D). The average CFSE fluorescence intensity was higher in PE^+CFSE^+ microglia from the $MyD88^{-/-}$ and $TLR4^{-/-}$ groups than in the microglia of the WT group (Fig. 5E), and significantly fewer RBCs were nonphagocytosed in the $MyD88^{-/-}$ and $TLR4^{-/-}$ groups (Fig. 5F). The phagocytic capacity of $MyD88^{-/-}$ and $TLR4^{-/-}$ microglia treated with anti-CD36 Abs was significantly inhibited; in contrast, the phagocytic capacity of $MyD88^{-/-}$ and $TLR4^{-/-}$ microglia treated with IgG was not affected (Fig. 5D–F). These results indicate that TLR4 signaling may downregulate CD36 expression and inhibit hematoma absorption.

The effect of inflammatory molecules released downstream of TLR4 signaling (such as TNF-α) on the phagocytic capacity of microglia was investigated. Western blot analysis showed that the addition of RBCs to microglial cultures in the presence of TNF-α and IL-1β significantly decreased CD36 expression; in contrast, the addition of IL-10 significantly upregulated CD36 expression (Fig. 6A). The microglia CD36 expression levels observed using flow cytometry were consistent with the above results (Fig. 6B). The percentage of PE^+CFSE^+ microglia in the TNF-α– and IL-1β–treated groups was lower than in the vehicle-treated group (Fig. 6C); additionally, the average fluorescence intensity of CFSE in PE^+CFSE^+ microglia was decreased (Fig. 6D) and the number of nonphagocytosed RBCs was increased (Fig. 7E) in the treated groups. In contrast, in the IL-10–treated group, the percentage of

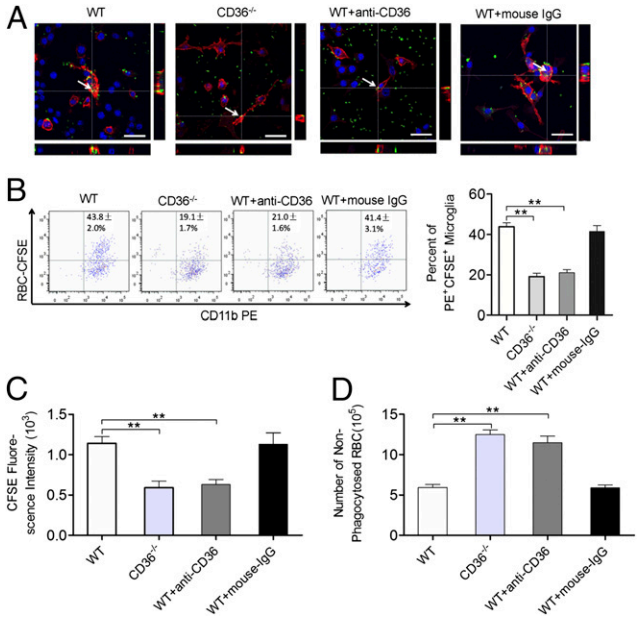

FIGURE 4. CD36-mediated engulfment of RBCs by microglia. (**A**) Observation of the phagocytosis of RBCs (CFSE-labeled, green) by microglia (Alexa Fluor 594–labeled, red) using confocal microscopy. The nuclei were stained with Hoechst. Serial sections along the *z*-axis were acquired and compiled as images. The *x*–*z*-axis is *below*, and the *y*–*z*-axis is on the *right*. The arrows indicate the RBCs engulfed by microglia. Scale bars, 40 μm. Detection of changes in the phagocytic ability of microglia using flow cytometry is shown. Microglia were stained with anti-mouse CD11b-PE and RBCs were stained with CFSE. (**B**) Representative flow cytometry plot (*left panel*) and the percentage of PE^+CFSE^+ microglia that had engulfed RBCs (*right panel*). (**C**) Average fluorescence intensity of CFSE in the PE^+CFSE^+ microglia. (**D**) The number of nonphagocytosed RBCs in the supernatant. $^{**}p < 0.01$ versus the WT microglia group, $n = 6$ for all graphs.

PE^+CFSE^+ microglia and the average fluorescence intensity of CFSE in PE^+CFSE^+ microglia increased and the number of nonphagocytosed RBCs decreased (Fig. 6C–E). These results suggest that molecules released downstream of TLR4 signaling (such as TNF-α and IL-1β) can inhibit hematoma absorption following ICH by downregulating CD36 expression.

TAK-242 increases CD36 expression, promotes hematoma absorption, and increases catalase expression

Our previous studies showed that TAK-242 could reduce secondary injury caused by ICH by inhibiting TLR4 signaling (14). To observe the effect of TAK-242 on hematoma absorption, CD36 expression levels were measured in microglia cocultured with RBCs in the presence of TAK-242, TAK-242 plus TNF-α, TAK-242 plus IL-1β, or vehicle (solution for TAK-242) for 12 h. Western blot analysis showed that CD36 expression levels were higher in the TAK-242 group than in the vehicle group, whereas the TAK-242–promoted expression of CD36 was weakened by TNF-α and IL-1β; TNF-α had an apparent effect in this process (Fig. 7A). However, when the microglia were treated with TAK-242 only, CD36 expression levels did not change significantly (data not shown). The CD36 expression changes determined by flow cytometry were consistent with the Western blot results (Fig. 7B). Flow cytometry showed that the percentage of PE^+CFSE^+ microglia in the TAK-242 group was increased (Fig. 7C); additionally, the average fluorescence intensity of CFSE in PE^+CFSE^+ microglia was increased (Fig. 7D), and the number of RBCs remaining in the supernatant was decreased (Fig. 7E). These findings suggest that TAK-242 can upregulate CD36 expression in microglia and promote RBC phagocytosis. In the TAK-242 plus TNF-α group and the TAK-242 plus IL-1β group, the percentage of PE^+CFSE^+ microglia and average fluorescence intensity of CFSE were reduced; however, the number of RBCs remaining in the supernatant was increased (Fig. 7C–E), and the effect of TNF-α was more apparent. These results suggest that the TLR4 signaling pathway regulates CD36 expression and its function via inflammatory factors, especially TNF-α. In the in vitro ICH model, the expression of catalase mRNA was significantly increased (Fig. 7F), and the H_2O_2 content was significantly decreased (Fig. 7G) in the microglia of the TAK-242 group. Finally, when TAK-242 was applied 6 h after the onset of the in vivo ICH models, the hematoma volume in treated mice was significantly lower than in mice of the vehicle control group 5 d after the onset of the hematoma. Because TNF-α had an inhibiting effect of CD36 expression in vitro, after the first injection of TAK-242, we immediately injected TNF-α, which showed that the protective effect could be weakened by TNF-α (Fig. 7H).

Discussion

Clinical trials evaluating the surgical removal of hematomas have not achieved the expected results (27). The promotion of hematoma absorption in cerebral tissues represents a new potential treatment option for patients with ICH (2, 3). However, the regulatory mechanism underlying hematoma absorption is still unclear. The present study showed that CD36-mediated hematoma absorption occurs in ICH patients and that this absorption is significantly associated with patient prognosis. The results of in vitro and in vivo experiments related to ICH further confirmed that CD36 promotes hematoma absorption. After the onset of ICH, inflammatory factors induced by the activation of the TLR4 signaling pathway downregulate CD36 expression and inhibit hematoma absorption. The application of TLR4 inhibitors could upregulate CD36 expression and increase hematoma absorption. To our knowledge, our study is the first to clarify the mechanism underlying hematoma absorption in patients with ICH; the results of this study provide reliable experimental data that may contribute to the development of clinical treatments that promote hematoma absorption in patients with ICH.

Two types of CD36 expression deficiency exist: patients with a type I deficiency have deficient CD36 expression in monocytes and platelets, and patients with a type II deficiency have deficient expression in platelets only (28). The cells from patients with a type I CD36 deficiency have a reduced ability to phagocytize oxidatively modified low-density lipoprotein; these patients often experience complications such as insulin resistance, hypertension, and the aggravation of atherosclerosis. Additionally, the incidence of coronary artery disease is three times higher in patients with a type I CD36 deficiency than in normal individuals (17). CD36 expression deficiencies are rarely encountered among European and American whites; however, >2% of Asians and Africans are afflicted with a CD36 deficiency, and the prevalence of this deficiency in Japan ranges from 3 to 11% (29, 30). We used a sequence-specific primer PCR assay to detect CD36 expression deficiencies in ICH patients. Sequencing and Western blot analyses identified 11 patients with a type I deficiency from among 199 patients (5.5%). The high prevalence of this deficiency in our patient population may be due to regional differences, small sample sizes, and the fact that only patients with ICH were selected. We found that type I CD36–deficient ICH patients had hematomas that were less well absorbed, and they had significantly more severe neurologic deficits than did patients with normal CD36 expression. These results suggest that CD36 pro-

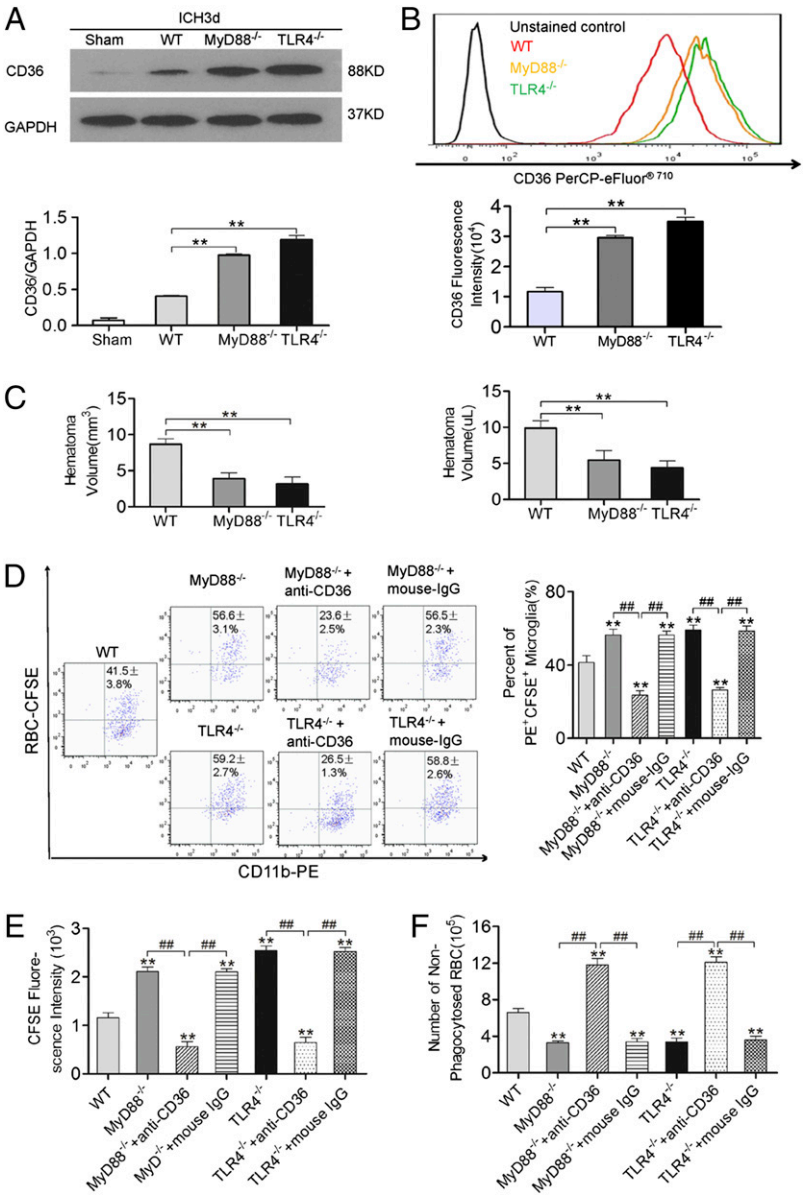

FIGURE 5. TLR4 signaling downregulates CD36 expression and increases hematoma absorption. (**A**) Detection of CD36 expression in perihematomal tissues 3 d after the onset of ICH using Western blot. $^{**}p < 0.01$ versus the WT group, $n = 6$. (**B**) Detection of microglia CD36 expression using flow cytometry. $^{**}p < 0.01$ versus the WT group, $n = 6$. (**C**) Five days after the onset of ICH, the hematoma volume was smaller in MyD88$^{-/-}$ and TLR4$^{-/-}$ mice than in WT mice. Measurement of hematoma volume using Image-Pro Plus (*left panel*) and hemoglobin detection (*right panel*) are shown. $^{**}p < 0.01$ versus the WT group, $n = 6$. Detection of changes in the phagocytic capacity of microglia using flow cytometry is depicted. Microglia were stained with anti-mouse CD11b-PE, and RBCs were stained with CFSE. (**D**) Representative flow cytometry plot (*left panel*) and the percentage of PE$^+$ CFSE$^+$ microglia that had engulfed RBCs (*right panel*); (**E**) average fluorescence intensity of CFSE in PE$^+$ CFSE$^+$ microglia; (**F**) number of nonphagocytosed RBCs in the supernatant. $^{**}p < 0.01$ versus the WT microglia group, $^{\#\#}p < 0.01$ versus the groups with anti-CD36 Abs, $n = 6$ for all flow cytometry graphs.

motes hematoma absorption after ICH and confirm that the rate at which the hematoma is absorbed positively correlated with patient prognosis. The destruction of the blood–brain barrier following ICH can allow peripheral mononuclear macrophages to enter perihematomal tissues (16); therefore, it has been suggested that the CD36$^+$ peripheral mononuclear macrophages that enter into the perihematomal tissues participate in hematoma absorption. Microglia are resident brain mononuclear macrophages; our data showed that CD36 was mainly expressed in microglia near the perihematomal tissues following ICH and that microglial CD36 played an important role in enabling hematoma absorption. These two types of cells are thought to play important roles in hematoma absorption; however, further studies are required to determine which cell type is more important. Additionally, because our study was conducted at a single center with a small sample size, our conclusions must be confirmed in multicenter studies with larger sample sizes. The relevant studies are currently in progress.

We found that CD36 significantly promotes hematoma absorption following ICH; however, the regulatory mechanism underlying this process remains unclear. Studies have shown that inflammatory factors such as TNF-α that are induced by TLR signaling can regulate the expression of CD36 in macrophages that are very important in infection-related inflammatory responses (15). This suggests that the activation of TLR4 signaling following ICH may have a negative regulatory effect on CD36 expression. Our study showed three significant results. First, CD36 expression was significantly upregulated in perihematomal tissues in TLR4$^{-/-}$ and MyD88$^{-/-}$ mice. Second, hematoma absorption was significantly increased in TLR4$^{-/-}$ and MyD88$^{-/-}$ mice. The microglia of TLR4$^{-/-}$ and MyD88$^{-/-}$ mice engulfed more RBCs than did WT microglia; however, after treatment with anti-CD36 Abs, the phagocytic ability of TLR4$^{-/-}$ and MyD88$^{-/-}$ microglia was significantly decreased, suggesting that TLR4 signaling regulated hematoma absorption through CD36. Third, the inflammatory factors TNF-α and IL-1β that were induced by the activation of TLR4 signaling downregulated microglial CD36 expression and inhibited hematoma absorption. These results suggest that CD36 mediates hematoma absorption; however, the activation of TLR4 signaling following ICH can activate NF-κB via the MyD88 pathway, resulting in the production of large amounts of TNF-α and IL-1β (13). TNF-α and IL-1β can inhibit CD36 expression and slow hematoma absorption. Sansing et al. (16) reported that CD36

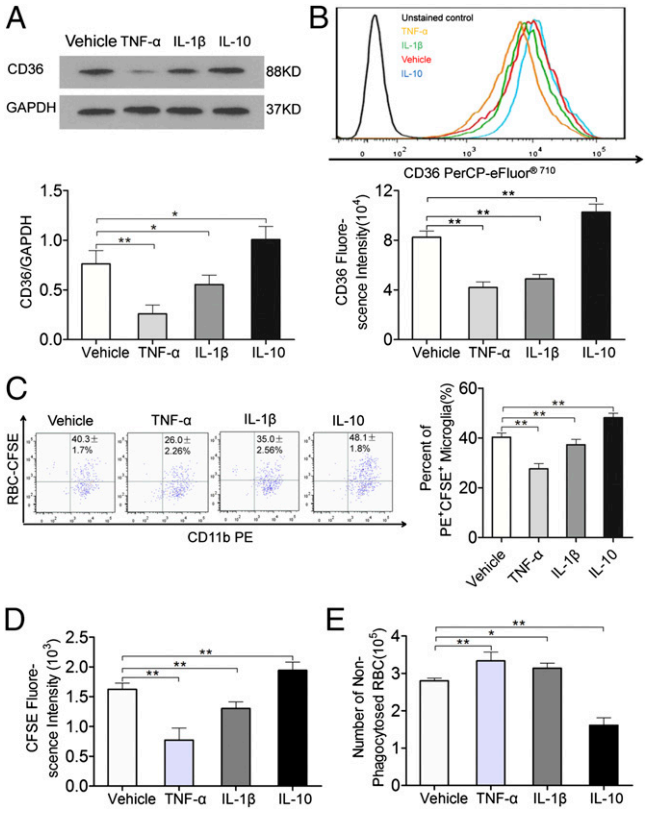

FIGURE 6. Effects of TNF-α, IL-1β, and IL-10 on CD36 expression and phagocytosis in microglia. (**A**) Detection of changes in microglial CD36 protein levels using Western blot. $*p < 0.05$ versus the vehicle group, $**p < 0.01$ versus the vehicle group, $n = 6$. (**B**) Detection of microglial CD36 expression using flow cytometry. $**p < 0.01$ versus the vehicle group, $n = 6$. Detection of changes in the phagocytic ability of microglia using flow cytometry. Microglia were stained with anti-mouse CD11b-PE, and RBCs were stained with CFSE. (**C**) Representative flow cytometry plot (*left panel*) and the percentage of PE^+CFSE^+ microglia that had engulfed RBCs (*right panel*). $**p < 0.01$ versus the vehicle group, $n = 6$. (**D**) Average fluorescence intensity of CFSE in PE^+CFSE^+ microglia. $**p < 0.01$ versus the vehicle group, $n = 6$. (**E**) Number of nonphagocytosed RBCs in the supernatant. $*p < 0.05$ versus the vehicle group, $**p < 0.01$ versus the vehicle group, $n = 6$.

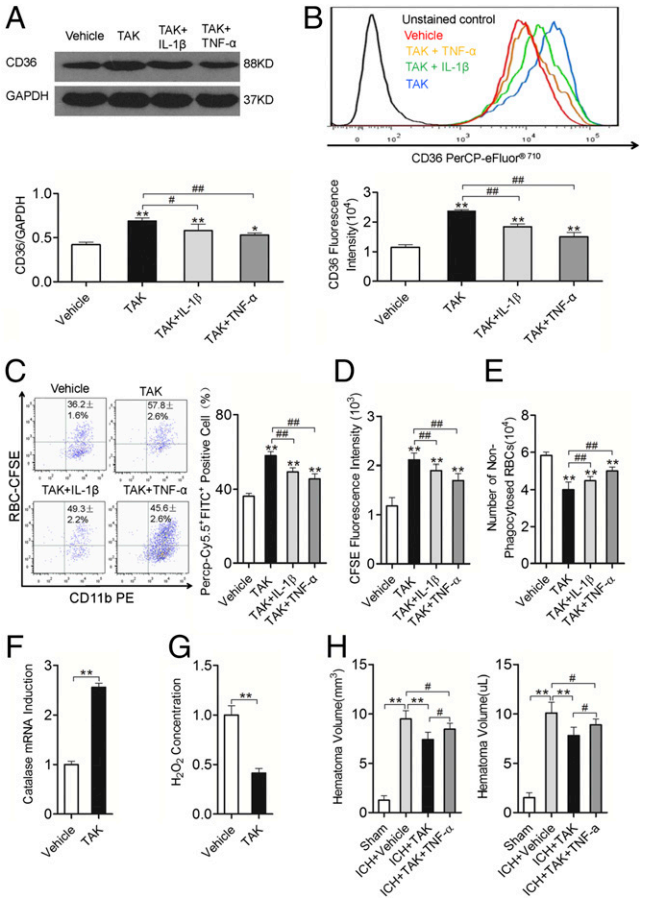

FIGURE 7. TAK-242 (TAK) increases CD36 expression and promotes hematoma absorption. (**A**) Detection of CD36 protein expression using Western blot. $**p < 0.01$ versus the vehicle group, $^{\#}p < 0.05$ versus the TAK group, $^{\#\#}p < 0.01$ versus the TAK group, $n = 6$. (**B**) Detection of microglia CD36 expression using flow cytometry. $**p < 0.01$ versus the vehicle group, $^{\#\#}p < 0.01$ versus the TAK group, $n = 6$. Detection of changes in the phagocytic capacity of microglia using flow cytometry. Microglia were stained with anti-mouse CD11b-PE, and RBCs were stained with CFSE. (**C**) A representative flow cytometry plot (*left panel*) displaying the percentage of PE^+CFSE^+ microglia (*right panel*) that had engulfed RBCs. $**p < 0.01$ versus the vehicle group, $^{\#\#}p < 0.01$ versus the TAK group, $n = 6$. (**D**) The average fluorescence intensity of CFSE in PE^+CFSE^+ microglia. $**p < 0.01$ versus the vehicle group, $^{\#\#}p < 0.01$ versus the TAK group, $n = 6$. (**E**) The number of nonphagocytosed RBCs in the supernatant. $**p < 0.01$ versus the vehicle group, $^{\#\#}p < 0.01$ versus the TAK group, $n = 6$. (**F**) Detection of microglial catalase expression using real-time quantitative RT-PCR. The data are expressed as fold increases relative to the vehicle group. $**p < 0.01$, $n = 6$. (**G**) The changes in H_2O_2 content in the supernatant were measured. The results are presented as fold changes relative to vehicle group. $**p < 0.01$, $n = 6$. (**H**) Changes in hematoma volume in mice at 5 d after the onset of ICH. Measurement of hematoma volume using Image-Pro Plus (*left panel*) and detection of hemoglobin (*right panel*). $**p < 0.01$ versus the ICH plus vehicle group, $^{\#}p < 0.05$ versus the ICH plus TAK plus TNF-α group, $n = 6$.

expression was upregulated in the TLR4 knockout mice following ICH, suggesting that TLR4 may have participated in the CD36 regulation, which was consistent with our results that TLR4 regulated the CD36 expression in the ICH. However, recent research suggests that under the stimulation of oxidized low-density lipoprotein and amyloid-β, CD36 functions as a TLR4/TLR6 coreceptor and participated in the early inflammatory mediators expression in atherosclerosis and Alzheimer disease (31). The reasons for differing results may be related to using different models, and CD36 may have different functions varying among diseases. Moreover, our results suggest that IL-10 can promote CD36 expression and enhance the ability of microglia to phagocytize RBCs; however, IL-10 levels were not obviously increased 1 and 3 d after ICH (32), suggesting that the protective role of IL-10 during the acute phase of cerebral hemorrhage was limited. Therefore, residual blood components activated TLR4 signaling and produced inflammatory injury, thus initiating an inflammatory cascade reaction and aggravating neurologic deficits. The inhibition of the activation of TLR4 signaling could therefore inhibit inflammatory responses and promote hematoma absorption.

Our recent studies have shown that the TLR4 inhibitor TAK-242 significantly relieves inflammatory injury after ICH and improves neurologic deficits (14). The present study further showed that TAK-242 upregulated CD36 expression in microglia, increasing the phagocytic capacity of microglia and improving hematoma absorption in ICH mice. However, simultaneous use of TNF-α and IL-1β could weaken the ability of TAK-242 to upregulate CD36 expression. This finding suggests that the TAK-242–mediated mechanism underlying the relief of inflammatory injury in mice

with ICH was associated with the promotion of hematoma absorption. The specific neuroprotection induced by TAK-242 was associated with the inhibition of TLR4 signaling and the upregulation of CD36 expression.

Phagocytosis is essential for hematoma absorption. However, the injury to perihematomal cells caused by inflammatory factors and oxygen-free radicals released during the phagocytosis of RBCs requires further attention (2). Our results show that TAK-242 promoted phagocytosis, increased catalase expression, and reduced H_2O_2 production. Therefore, the promotion of hematoma absorption by TAK-242 did not result in a concomitant increase in the production of free radicals or damage to perihematomal tissues. This finding confirms that TAK-242 represents a potentially viable treatment option for patients with ICH. Because TLR4 plays an important role in the immune response, complete inhibition of TLR4 would not be appropriate for all scenarios. Our research moderately regulated TLR4 to restrain excessive inflammation; subsequent research regarding the regulation of the TLR4 signaling pathway is under way.

Disclosures

The authors have no financial conflicts of interest.

References

1. Keep, R. F., Y. Hua, and G. Xi. 2012. Intracerebral haemorrhage: mechanisms of injury and therapeutic targets. *Lancet Neurol.* 11: 720–731.
2. Zhao, X., G. Sun, J. Zhang, R. Strong, W. Song, N. Gonzales, J. C. Grotta, and J. Aronowski. 2007. Hematoma resolution as a target for intracerebral hemorrhage treatment: role for peroxisome proliferator-activated receptor γ in microglia/macrophages. *Ann. Neurol.* 61: 352–362.
3. Zhao, X., J. Grotta, N. Gonzales, and J. Aronowski. 2009. Hematoma resolution as a therapeutic target: the role of microglia/macrophages. *Stroke* 40(3, Suppl. 1): S92–S94.
4. Fang, H., P. F. Wang, Y. Zhou, Y. C. Wang, and Q. W. Yang. 2013. Toll-like receptor 4 signaling in intracerebral hemorrhage-induced inflammation and injury. *J. Neuroinflammation* 10: 27.
5. Nyquist, P. 2010. Management of acute intracranial and intraventricular hemorrhage. *Crit. Care Med.* 38: 946–953.
6. Husemann, J., J. D. Loike, R. Anankov, M. Febbraio, and S. C. Silverstein. 2002. Scavenger receptors in neurobiology and neuropathology: their role on microglia and other cells of the nervous system. *Glia* 40: 195–205.
7. Fadok, V. A., M. L. Warner, D. L. Bratton, and P. M. Henson. 1998. CD36 is required for phagocytosis of apoptotic cells by human macrophages that use either a phosphatidylserine receptor or the vitronectin receptor ($\alpha_v\beta_3$). *J. Immunol.* 161: 6250–6257.
8. McGilvray, I. D., L. Serghides, A. Kapus, O. D. Rotstein, and K. C. Kain. 2000. Nonopsonic monocyte/macrophage phagocytosis of *Plasmodium falciparum*-parasitized erythrocytes: a role for CD36 in malarial clearance. *Blood* 96: 3231–3240.
9. Febbraio, M., D. P. Hajjar, and R. L. Silverstein. 2001. CD36: a class B scavenger receptor involved in angiogenesis, atherosclerosis, inflammation, and lipid metabolism. *J. Clin. Invest.* 108: 785–791.
10. Ren, Y., R. L. Silverstein, J. Allen, and J. Savill. 1995. CD36 gene transfer confers capacity for phagocytosis of cells undergoing apoptosis. *J. Exp. Med.* 181: 1857–1862.
11. Takeuchi, O., and S. Akira. 2010. Pattern recognition receptors and inflammation. *Cell* 140: 805–820.
12. Okun, E., K. J. Griffioen, and M. P. Mattson. 2011. Toll-like receptor signaling in neural plasticity and disease. *Trends Neurosci.* 34: 269–281.
13. Lin, S., Q. Yin, Q. Zhong, F. L. Lv, Y. Zhou, J. Q. Li, J. Z. Wang, B. Y. Su, and Q. W. Yang. 2012. Heme activates TLR4-mediated inflammatory injury via MyD88/TRIF signaling pathway in intracerebral hemorrhage. *J. Neuroinflammation* 9: 46.
14. Wang, Y. C., P. F. Wang, H. Fang, J. Chen, X. Y. Xiong, and Q. W. Yang. 2013. Toll-like receptor 4 antagonist attenuates intracerebral hemorrhage-induced brain injury. *Stroke* 44: 2545–2552.
15. Zamora, C., E. Cantó, J. C. Nieto, M. Angels Ortiz, C. Juarez, and S. Vidal. 2012. Functional consequences of CD36 downregulation by TLR signals. *Cytokine* 60: 257–265.
16. Sansing, L. H., T. H. Harris, F. A. Welsh, S. E. Kasner, C. A. Hunter, and K. Kariko. 2011. Toll-like receptor 4 contributes to poor outcome after intracerebral hemorrhage. *Ann. Neurol.* 70: 646–656.
17. Janabi, M., S. Yamashita, K. Hirano, N. Sakai, H. Hiraoka, K. Matsumoto, Z. Zhang, S. Nozaki, and Y. Matsuzawa. 2000. Oxidized LDL-induced NF-κB activation and subsequent expression of proinflammatory genes are defective in monocyte-derived macrophages from CD36-deficient patients. *Arterioscler. Thromb. Vasc. Biol.* 20: 1953–1960.
18. Yuasa-Kawase, M., D. Masuda, T. Yamashita, R. Kawase, H. Nakaoka, M. Inagaki, K. Nakatani, K. Tsubakio-Yamamoto, T. Ohama, A. Matsuyama, et al. 2012. Patients with CD36 deficiency are associated with enhanced atherosclerotic cardiovascular diseases. *J. Atheroscler. Thromb.* 19: 263–275.
19. Kidwell, C. S., and M. Wintermark. 2008. Imaging of intracranial haemorrhage. *Lancet Neurol.* 7: 256–267.
20. Kazui, S., H. Naritomi, H. Yamamoto, T. Sawada, and T. Yamaguchi. 1996. Enlargement of spontaneous intracerebral hemorrhage. Incidence and time course. *Stroke* 27: 1783–1787.
21. Kothari, R. U., T. Brott, J. P. Broderick, W. G. Barsan, L. R. Sauerbeck, M. Zuccarello, and J. Khoury. 1996. The ABCs of measuring intracerebral hemorrhage volumes. *Stroke* 27: 1304–1305.
22. Lyden, P. D., A. Shuaib, K. R. Lees, A. Davalos, S. M. Davis, H. C. Diener, J. C. Grotta, T. J. Ashwood, H. G. Hardemark, H. H. Svensson, et al; CHANT Trial Investigators. 2007. Safety and tolerability of NXY-059 for acute intracerebral hemorrhage: the CHANT Trial. *Stroke* 38: 2262–2269.
23. Rać, M. E., K. Safranow, and W. Poncyljusz. 2007. Molecular basis of human CD36 gene mutations. *Mol. Med.* 13: 288–296.
24. Kashiwagi, H., Y. Tomiyama, S. Nozaki, T. Kiyoi, S. Tadokoro, K. Matsumoto, S. Honda, S. Kosugi, Y. Kurata, and Y. Matsuzawa. 2001. Analyses of genetic abnormalities in type I CD36 deficiency in Japan: identification and cell biological characterization of two novel mutations that cause CD36 deficiency in man. *Hum. Genet.* 108: 459–466.
25. Yang, Q. W., F. L. Lu, Y. Zhou, L. Wang, Q. Zhong, S. Lin, J. Xiang, J. C. Li, C. Q. Fang, and J. Z. Wang. 2011. HMBG1 mediates ischemia-reperfusion injury by TRIF-adaptor independent Toll-like receptor 4 signaling. *J. Cereb. Blood Flow Metab.* 31: 593–605.
26. Loftspring, M. C., H. L. Johnson, R. Feng, A. J. Johnson, and J. F. Clark. 2011. Unconjugated bilirubin contributes to early inflammation and edema after intracerebral hemorrhage. *J. Cereb. Blood Flow Metab.* 31: 1133–1142.
27. Mendelow, A. D., B. A. Gregson, E. N. Rowan, G. D. Murray, A. Gholkar, and P. M. Mitchell; STICH II Investigators. 2013. Early surgery versus initial conservative treatment in patients with spontaneous supratentorial lobar intracerebral haematomas (STICH II): a randomised trial. *Lancet* 382: 397–408.
28. Yamamoto, N., N. Akamatsu, H. Sakuraba, H. Yamazaki, and K. Tanoue. 1994. Platelet glycoprotein IV (CD36) deficiency is associated with the absence (type I) or the presence (type II) of glycoprotein IV on monocytes. *Blood* 83: 392–397.
29. Aitman, T. J. 2001. CD36, insulin resistance, and coronary heart disease. *Lancet* 357: 651–652.
30. Yamamoto, N., H. Ikeda, N. N. Tandon, J. Herman, Y. Tomiyama, T. Mitani, S. Sekiguchi, R. Lipsky, U. Kralisz, and G. A. Jamieson. 1990. A platelet membrane glycoprotein (GP) deficiency in healthy blood donors: Naka- platelets lack detectable GPIV (CD36). *Blood* 76: 1698–1703.
31. Stewart, C. R., L. M. Stuart, K. Wilkinson, J. M. van Gils, J. Deng, A. Halle, K. J. Rayner, L. Boyer, R. Zhong, W. A. Frazier, et al. 2010. CD36 ligands promote sterile inflammation through assembly of a Toll-like receptor 4 and 6 heterodimer. *Nat. Immunol.* 11: 155–161.
32. Wasserman, J. K., X. Zhu, and L. C. Schlichter. 2007. Evolution of the inflammatory response in the brain following intracerebral hemorrhage and effects of delayed minocycline treatment. *Brain Res.* 1180: 140–154.